Transmission electron microscopy study of ion tracks in nanocrystalline $Y_3Fe_5O_{12}$

A. Mutali[1,2,*], M. Badenhorst[3], J. O'Connell[3],
R. Rymzhanov[1,2], V. Skuratov[2,4,5]

[1]Institute of Nuclear Physics, Almaty, Kazakhstan

[2]Joint Institute for Nuclear Research, Dubna, Russia

[3]Centre for High Resolution Transmission Electron Microscopy,
Nelson Mandela University, Port Elizabeth, South Africa

[4]Institute of Nuclear Physics and Engineering,
National Research Nuclear University MEPhI, Moscow, Russia

[5]Department of Nuclear Physics, Dubna State University, Dubna, Russia

e-mail: mutali@jinr.ru

Abstract

Transmission electron microscopy (TEM) was used to study the structural effects in nanocrystalline yttrium-iron garnet ($Y_3Fe_5O_{12}$, YIG) induced by swift heavy ions (SHI). The nanopowder specimens were irradiated with Bi and Xe ions with energies from 230 to 670 MeV and fluences in the range of 2×10^{11} to 5×10^{12} ion/cm^2 with and without different thickness aluminium degraders. Ion impacts in nanoparticles induce the formation of amorphous cylindrical tracks similar to those previously observed in the bulk. The track size was found to be slightly larger in the vicinity of nanocrystals edges due to surface effects. The threshold energy loss for track formation was estimated in the range 4.6–6.92 keV/nm, while no tracks were detected at S_e lower than 4.6 keV/nm. These results contribute to the understanding of radiation-induced damage processes in nanocrystalline materials and provide useful insight into track formation mechanisms in complex oxides under high electronic excitation.

1   Introduction

Heavy ions traveling through matter lose energy via two main mechanisms: elastic collisions with target atom nuclei (nuclear stopping power) and interactions with target electrons (electronic stopping power). At higher ion energies (~ 0.5 MeV/amu, swift heavy ions, SHI), most of the energy is dissipated through ionization and electronic excitations. In insulating materials, this electronic energy is localized and transferred to the lattice atoms within 5–10 nm of the ion trajectory, leading to significant structural damage along the ion's path, forming what is known as a latent track. Taking advantage of these characteristics, swift heavy ion irradiation is regarded as a distinctive method for nanostructuring solid materials and has already been applied in a range of practical uses [1–4]. Ion tracks are employed to modify the magnetic and magneto-optical properties of garnets, enabling their use in technological applications such as data storage media.

Over the past few decades, the effects of swift heavy ion irradiation on $Y_3Fe_5O_{12}$ (YIG) have been extensively studied. Several works have revealed formation of amorphous tracks after irradiation with SHIs [5, 6]. Evaluation of track size and structural variation with ion energy and velocity demonstrated a complex relationship between energy loss and the track formation. For a specific type of projectile, the track diameter grows as the ion velocity increases, reaches a maximum, and then decreases once the velocity surpasses the stopping power peak, resulting in the characteristic "hook-like" curves [6]. This phenomenon, commonly referred to as the "velocity effect" indicates that for the same energy loss, slower projectiles produce tracks with larger diameters than faster ones, owing to differences in how densely energy is deposited by ions at low versus high velocities. Irradiation of the YIG surface with 200 MeV Au ions led to the formation of amorphous hillocks [7] on top of amorphous tracks.

Unlike bulk materials and microstructures, isolated nanoscale objects can respond in distinctive ways to the high ionization density produced by swift heavy ions. Recent experimental studies have explored size-dependent effects in systems such as nanocrystalline solids, thin films, and nanowires under high-energy ion irradiation [8–14]. However, research on the structural impact of swift heavy ions on free-standing nanoparticles [15–17] remains limited. It has been shown that the threshold ionization energy required to induce defects strongly depends on the size of the nanoparticles. Such size-related effects are observed for particles up to about 30–50 nm, suggesting that track formation is significantly influenced by nearby free surfaces. At the same time, the need for a deeper understanding of how excess energy is spatially confined within these nanoscale systems under SHI excitation calls for detailed investigation involving precise experimental techniques.

This motivated the present experimental study aimed at understanding how swift heavy ion irradiation modifies YIG nanoparticles as a function of their size and ion energy. The nanopowders deposited on substrate grid were irradiated with high energy heavy ions and examined using high-resolution transmission electron microscopy in order to observe SHI damage morphology.

2   Materials and Methods

Commercial nanocrystalline (nc) YIG powder was purchased from Sigma-Aldrich. Prior to irradiation, the samples were prepared for TEM analysis. Although the preparation procedure was identical for all specimens, centrifugation parameters were varied. The nanopowder was first weighed and then ground using an agate mortar and pestle to reduce agglomeration. Thereafter, the powder was placed into a test tube and dispersed in ethanol. The suspension was treated in a Bandelin ultrasonic bath, followed by an additional few minutes of dispersion using a mechanical disperser. After ultrasonic treatment, a centrifuge was used to perform sedimentation, separating particles into fractions. The resulting dispersions were deposited onto carbon-coated copper TEM grids for further irradiation and TEM analysis. The grid was then air-dried at room temperature.

Irradiation experiments were performed at room temperature using the U-400 cyclotron at the Flerov Laboratory of Nuclear Reactions of the Joint Institute for Nuclear Research (Dubna, Russia), and DC-60 cyclotron at Astana Branch of Institute of Nuclear Physics (Astana, Kazakhstan). The samples were irradiated with 670 MeV Bi, 230 and 475 MeV Xe ions in the fluence range from 2×10^{11} to 5×10^{12} ion/cm^2 with a fluence measurement accuracy of about 10%. Aluminium (Al) degraders with thicknesses between 8.02 μm to 36.4 μm were used to modify the ion energies. The electronic stopping power (S_e) was estimated using SRIM-2016.

Structural analysis of the nanoparticles before and after irradiation was conducted using a transmission electron microscopy FEI Talos™ F200i S/TEM operating at 200 kV. Image analysis was performed using Velox and Gatan Digital Micrograph software. Track parameters were measured from bright-field (BF), dark-field (DF), and high-resolution TEM (HRTEM) images. This approach relies on the contrast between the tracks and the nanoparticles in the TEM images to discern the tracks as circular features with sharp boundaries. In practice, track radius measurements have some degree of uncertainty due to diffraction effects producing contrast unrelated to the ion tracks, especially for irregularly shaped tracks.

3   Results and Discussion

Fig. 1a and b show TEM images of the initial specimens, providing an overview of the particle morphology and their spatial distribution. At low magnification, the material appears as an assembly of numerous nanoparticles dispersed over the support film, frequently forming agglomerates. Higher-magnification images reveal that the particles are close to spherical in shape. The average size of the nanoparticles is estimated to be in the range of approximately 8–15 nm, which corresponds to nanoscale YIG crystallites. In addition to these, larger clusters with sizes of 40–70 nm are occasionally observed. It can also be observed that some nanoparticles exhibit well-defined faceting, predominantly hexagonal with strong diffraction contrast, while others clearly reveal the crystalline features.
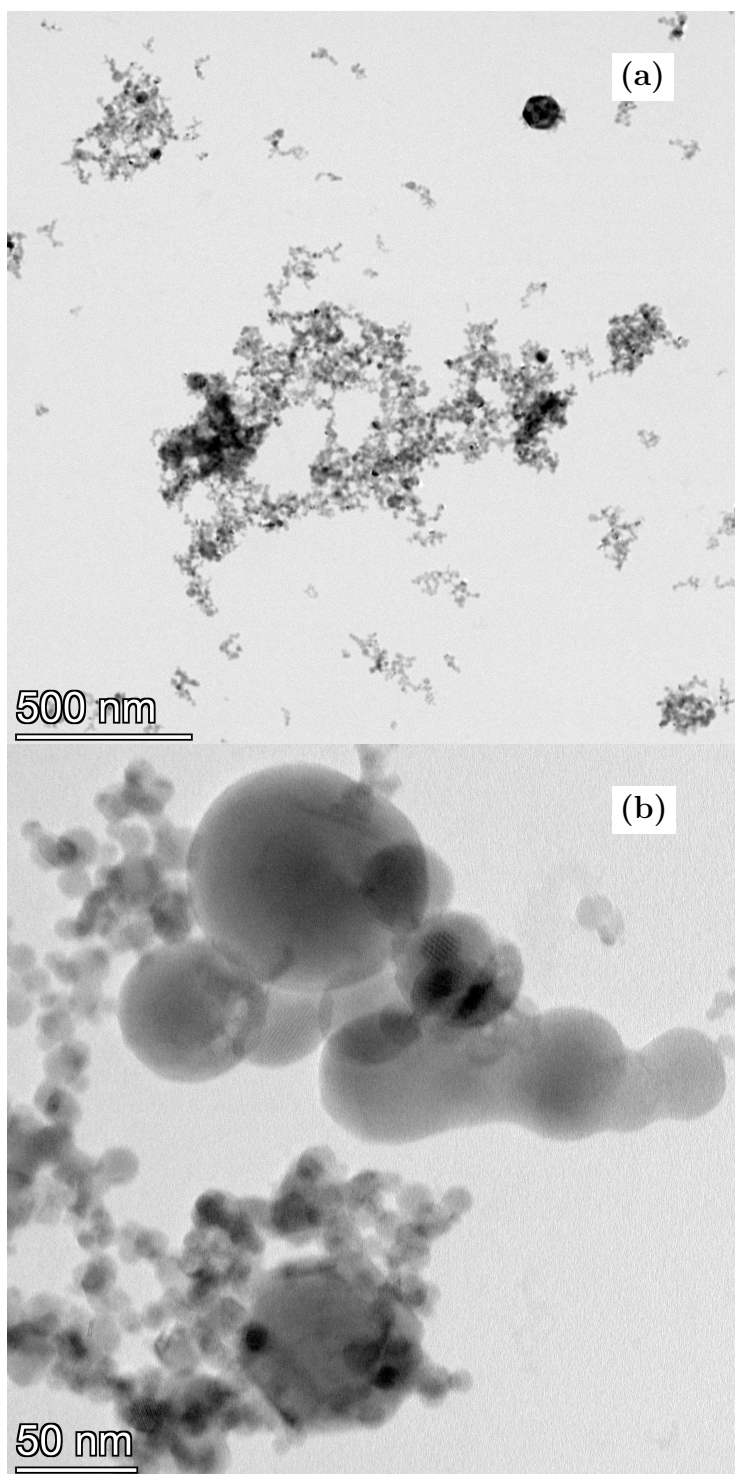
Figure 1: TEM images of nc-YIG nanoparticles deposited onto a carbon support film: (a) low and (b) high magnification.

Once the electronic stopping power exceeds a specific threshold value, ion tracks are formed from high-energy Xe and Bi ions. This is evident through the investigation of bright field (BF) and dark field (DF) TEM images of irradiated nc-YIG specimens by 670 MeV Bi, 475 MeV and 230 MeV Xe ions with different aluminium degraders as shown in Fig. 2. It is clear from Fig. 2, that the morphology of the tracks appears circular, representing cross sections of the amorphous cylindrical ion tracks [18]. The tracks could be identified and distinguished from the surrounding nanoparticles by

their uniform intensity and the absence of diffraction contrast and lattice fringes inside their cores, as indicated by the red boxes in Fig. 2(a) and (d). The track radii were measured using the line tool in Velox, as depicted by the red line in Fig. 2(a) across the crystalline-amorphous boundary. To ensure consistency, only distinct, non-overlapping tracks were measured. From the DF images, Fig. 2(c) and (d), the crystalline regions are perceived as bright regions. In contrast, due to their amorphous nature (absence of strong diffraction), the tracks are perceived as dark regions.
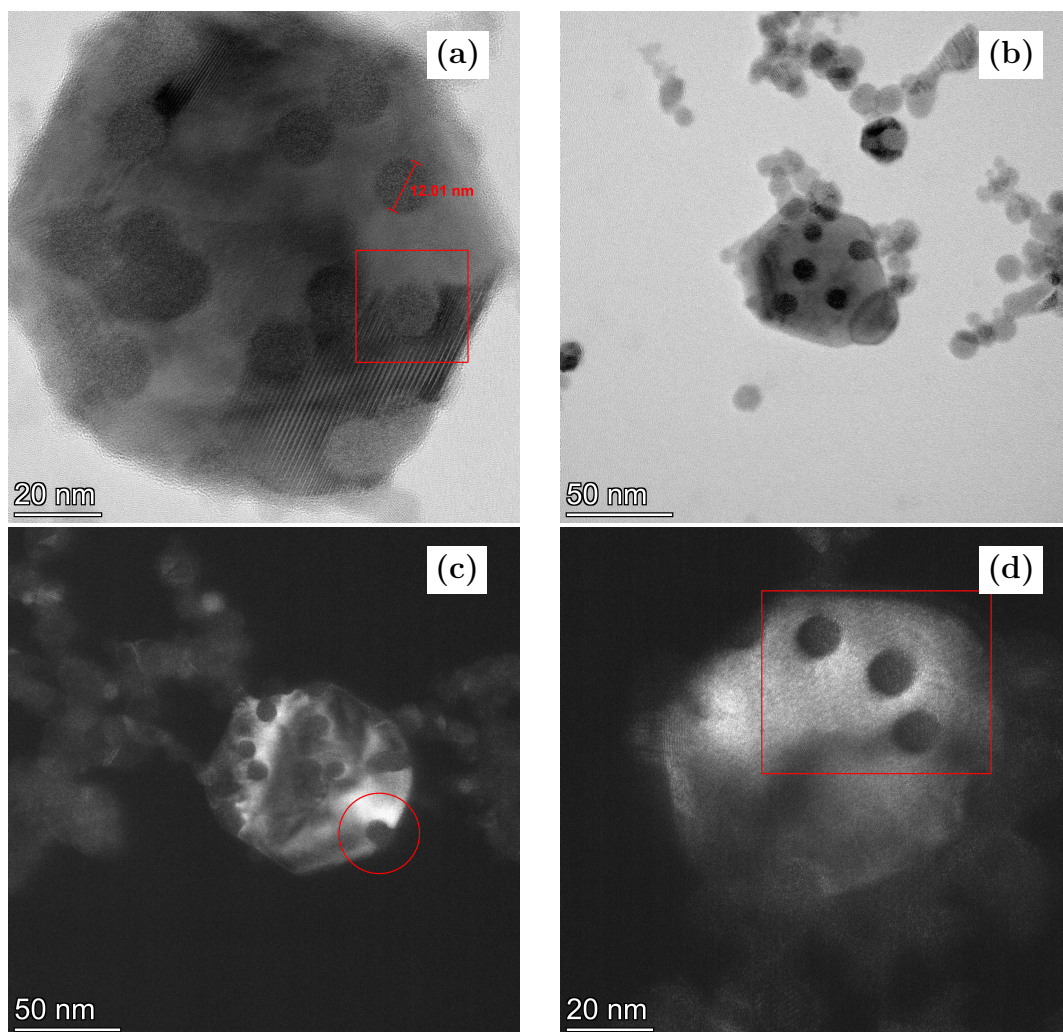

Figure 2: BF TEM images of nc-YIG irradiated with (a) Bi ($S_e = 34.32 \pm 0.11$ keV/nm) and (b) Xe ($S_e = 26.64 \pm 0.04$ keV/nm) as well as DF TEM images irradiated with (c) Xe ($S_e = 25.61 \pm 0.11$ keV/nm), and (d) Xe ($S_e = 21.91 \pm 0.16$ keV/nm) ions, each to a fluence of 2×10^{11} cm^{-2}. The red line represents a typical diameter measurement, the red boxes depict the contrast between an amorphous track and crystalline nanoparticle, and the red circle indicates the amorphous defects present at the border of the particles.

As annotated by the red circle in Fig. 2(c), it is evident that larger tracks are present near or on the border of the particles since it is thinner in projection than areas closer to the middle of the particle. Hence, these tracks on the borders of the particles were excluded from the measurements. Furthermore, degrader

thicknesses of 36.4 μm ($S_e = 4.63 \pm 0.30$ keV/nm) for 670 MeV Bi ions and 33.8 μm ($S_e = 2.82 \pm 0.43$ keV/nm) for 475 MeV Xe ions, were also excluded due to the absence of visible tracks or the insufficient number of observable tracks. The nc-YIG specimens were also irradiated with 230 MeV Xe ions to a fluence of 2×10^{12} cm^{-2} and 5×10^{12} cm^{-2}. At higher fluences there was a significant amount of track overlap, and a corresponding increase in uncertainty in determining the track borders. It was observed that the nanoparticles have become amorphous at these fluences due to the overlap of amorphous ion tracks.

The quality of the TEM images was influenced by several factors; therefore, only images with high contrast and good focus were selected. BF imaging mode could impose some restrictions on differentiating between the tracks and the nanoparticles. BF imaging mode could be utilised as shown in Fig. 2(b) as some tracks were clearly visible. However, it is suggested for future studies to base the track measurements on high-angular dark-field scanning transmission electron microscopy (HAADF STEM) images to enhance the contrast independent of the local diffraction condition and thus improve the consistency of the measurements [19, 20]. HAADF STEM imaging relies on the assumption that the specimen thickness and chemical composition are uniform, generally only valid for the small area within the field of view, and its contrast is related to the projected average atomic number of the specimen [19].

The results for the track measurements as well as the details of the irradiation parameters were tabulated in Table 1. These results include the initial ion energies, the thicknesses of Al degraders. The S_e values were determined through SRIM-2016 and the density of YIG was considered as 5.17 g/cm^3. The energy straggle of the incident ion beam after it traversed through the Al degrader. The energy dispersion of the initial ion beam was not considered.

Table 1: Ion irradiation parameters and track radii in nanocrystalline YIG.

Ion energy (MeV)	Al degrader thickness (μm)	Ion energy (MeV/amu)	S_e (keV/nm)	Track radius (nm)
Bi, 670	None	3.2	41.19	5.34 ± 0.44
	15.85 ± 0.15	1.34 ± 0.01	34.32 ± 0.11	6.07 ± 0.70
	22.05 ± 0.22	0.76 ± 0.01	27.43 ± 0.17	5.45 ± 0.48
	32.82 ± 0.29	0.14 ± 0.01	9.35 ± 0.43	2.12 ± 0.53
Xe, 475	None	3.59	28.94	4.19 ± 0.69
	13.66 ± 0.12	1.74 ± 0.016	26.64 ± 0.04	4.43 ± 0.59
	18.10 ± 0.21	1.44 ± 0.03	25.61 ± 0.11	4.20 ± 0.49
	22.05 ± 0.22	0.77 ± 0.01	21.30 ± 0.13	4.13 ± 0.55
	25.77 ± 0.28	0.43 ± 0.03	16.69 ± 0.55	3.73 ± 0.48
	28.74 ± 0.43	0.23 ± 0.02	11.4 ± 0.78	3.19 ± 0.45
	30.5 ± 0.27	0.14 ± 0.02	7.82 ± 0.70	2.16 ± 0.62
Xe, 230	None	1.74	26.66	4.35 ± 0.49
	8.02 ± 0.17	0.8 ± 0.02	21.91 ± 0.16	4.47 ± 0.41
	11.74 ± 0.25	0.47 ± 0.02	17.51 ± 0.37	4.03 ± 0.24
	14.03 ± 0.14	0.30 ± 0.01	13.57 ± 0.26	3.51 ± 0.35
	17.4 ± 0.19	0.12 ± 0.01	6.92 ± 0.36	2.03 ± 0.58

It is expected that the track radius should increase with increasing ion energy because faster SHIs have higher stopping power (up to Bragg peak), deposit more

energy to the target and consequently induce larger track radii. However, while this is the general trend of the data, there are some outliers. Track radii are consistently larger for 230 MeV Xe ions than for the 475 MeV Xe ions at similar S_e (after degrader). Table 1 summarizes track sizes deduced from analysis of TEM micrographs. Bi and Xe ion energies, specific ionizing energy loss and thickness of Al degraders are also given. The ranges provide a more comprehensive representation of the track size distribution as solely relying on the mean could result in misinterpretation of the variability and spread of the data. To ensure representative and reliable results, multiple measurements were taken for each degrader. Ten measurements were performed at different locations on each degrader, and the average value was calculated to represent the thickness. The standard deviation of these measurements was used to estimate the uncertainty associated with each thickness value.

Typically, smaller particles exhibit larger tracks at lower S_e values [21]. Specific energy loss could vary significantly at different positions along the ion path for individual ions since the transfer of ion energy is a stochastic process [21]. The relationship between the average track radii and the electronic stopping power, for all the irradiation conditions is graphically represented in Fig. 3.
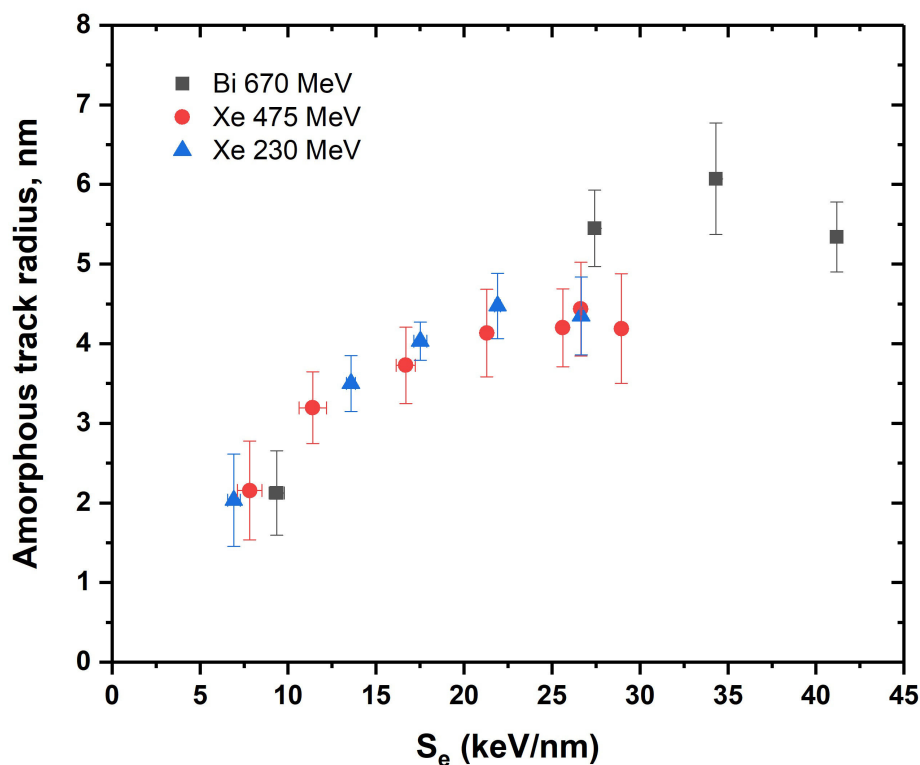

Figure 3: Variation of the average track radius with electronic stopping power.

In Fig. 3, it is observed that the greater the electronic stopping power value, the greater the average track radius, except for the last data point observed for 670 MeV Bi, 475 MeV and 230 MeV Xe ions which displays a lower track size. This phenomenon is the manifestation of the so-called "velocity effect" when faster ions (close or above Bragg peak energy) create more energetic electrons which results in a broader distribution of energy depositions. Faster electrons bring part of the deposited energy out of the track core reducing heating of the lattice and track

radius. Fig. 3 reveals that the results deviate from previous studies [22], but there is a resemblance in the dependence of track radius on S_e between the data points for 230 MeV Xe ions and the data points from previous studies [23], which reported a positive correlation between amorphous track radii and electronic stopping power.

Fig. 4 shows TEM images of nc-YIG irradiated with 230 MeV Xe ions at fluences of 2×10^{12} cm^{-2} and 5×10^{12} cm^{-2}. The corresponding SAED patterns are shown in the insets. At a fluence of 2×10^{12} cm^{-2} overlapping of ion tracks is clearly observed, which leads to the formation of disordered regions in the nanoparticles. The TEM images show an inhomogeneous contrast, indicating the presence of both amorphous and crystalline areas. This is also seen in the SAED pattern, where rings typical of an amorphous phase appear together with weak crystalline reflections. In some regions lattice fringes are still visible, suggesting that the crystalline structure is only partially damaged at this fluence. At a fluence of 5×10^{12} cm^{-2}, further accumulation and overlap of tracks result in complete amorphization of the nanoparticles. The TEM images become more homogeneous, with no visible lattice fringes and the SAED pattern contains only diffuse rings. With increasing fluence, the material transforms from a partially disordered state to a fully amorphous one.
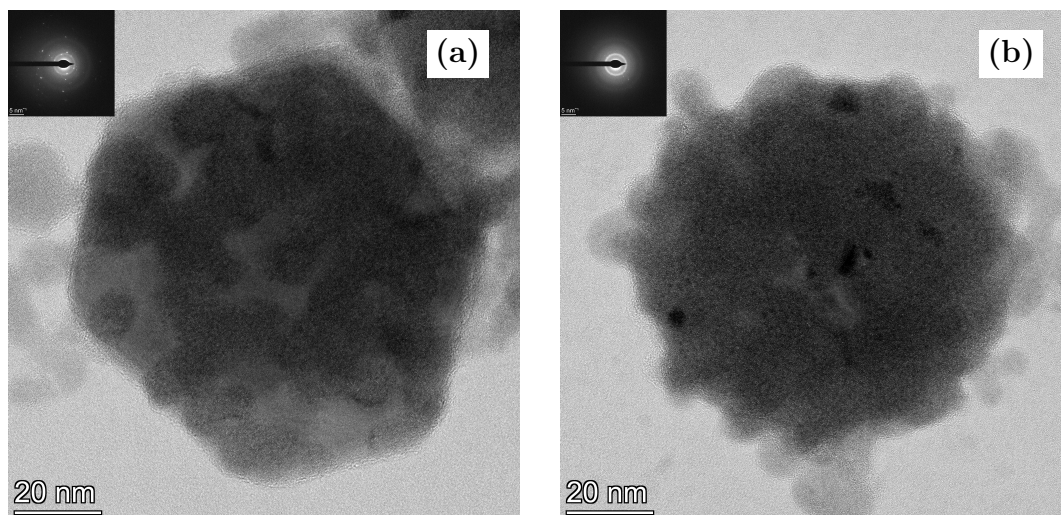

Figure 4: BF TEM images of nc-YIG irradiated with 230 MeV Xe ions at a fluence of (a) 2×10^{12} cm^{-2} and (b) 5×10^{12} cm^{-2} with SAED patterns.

4 Conclusions

TEM analysis was employed to measure the track radii of high energy Xe and Bi ions in nc-YIG. Amorphous ion tracks were formed at electronic stopping powers ranging from 6.92 to 41.19 keV/nm. At high fluences such as 5×10^{12} cm^{-2}, track overlap was observed and the nanoparticles appeared to transform into an amorphous material. Understanding the specific mechanisms of SHI-induced damage is crucial for the development and selection of inert matrix fuel hosts in nuclear applications as well as to investigate the responses of different materials to radiation damage. Therefore, future ion irradiation studies should focus on examining the response of nanocrystalline YIG specimens under various radiation conditions.

Acknowledgements

References

[1] K. K. Jana, B. Ray, D. K. Avasthi *et al.*, J. Mater. Chem. **22**, 3955 (2012).

[2] W. Wesch, E. Wendler, *Ion Beam Modification of Solids* (Springer, 2016).

[3] J. Zeng, J. Liu, S. Zhang *et al.*, Carbon **154**, 244 (2019).

[4] M. Rauber, I. Alber, S. Möller *et al.*, Nano Lett. **11**, 2304 (2011).

[5] A. Meftah, F. Brisard, J. M. Costantini *et al.*, Phys. Rev. B **48**, 920 (1993).

[6] J. Jensen, A. Dunlop, S. Della-Negra *et al.*, Nucl. Instrum. Methods Phys. Res. B **146**, 412 (1998).

[7] N. Ishikawa, T. Taguchi, N. Okubo, Nanotechnology **28**, 445708 (2017).

[8] S. Hémon, C. Dufour, F. Gourbilleau *et al.*, Nucl. Instrum. Methods Phys. Res. B **146**, 443 (1998).

[9] W. F. Cureton, R. I. Palomares, J. Walters *et al.*, Acta Mater. **160**, 47 (2018).

[10] P. Kalita, S. Ghosh, G. Gutierrez *et al.*, Sci. Rep. **11**, 10886 (2021).

[11] N. A. Nebogatikova, I. V. Antonova, S. V. Erohin *et al.*, Nanoscale **10**, 14499 (2018).

[12] A. A. Leino, O. H. Pakarinen, F. Djurabekova *et al.*, Nucl. Instrum. Methods Phys. Res. B **282**, 76 (2012).

[13] R. M. Papaléo, R. Thomaz, L. I. Gutierres *et al.*, Phys. Rev. Lett. **114**, 118302 (2015).

[14] D. Gehlawat, R. P. Chauhan, Mater. Chem. Phys. **145**, 60 (2014).

[15] A. Ibrayeva, J. O'Connell, A. Mutali *et al.*, Vacuum **233**, 113958 (2025).

[16] A. Ibrayeva, J. O'Connell, A. Mutali *et al.*, Crystals **13**, 1534 (2023).

[17] S. Stichleutner, B. Herczeg, J. Pechoušek *et al.*, Metals **14**, 421 (2024).

[18] A. Ibrayeva, A. Mutali, J. O'Connell *et al.*, Nucl. Mater. Energy **30**, 101106 (2022).

[19] A. Janse van Vuuren, A. Ibrayeva, R. A. Rymzhanov *et al.*, Mater. Res. Express **7**, 025512 (2020).

[20] A. Janse van Vuuren, A. Mutali, A. Ibrayeva *et al.*, Crystals **12**, 1410 (2022).

[21] A. Ibrayeva, J. O'Connell, A. Mutali *et al.*, Crystals **13**, 1534 (2023).

[22] M. M. Saifulin, J. H. O'Connell, A. J. Van Vuuren *et al.*, Nucl. Instrum. Methods Phys. Res. B **460**, 98 (2019).

[23] J. Jensen, A. Dunlop, S. Della-Negra *et al.*, Nucl. Instrum. Methods Phys. Res. B **146**, 412 (1998).